CHEMISTRY OF MATERIALS

pubs.acs.org/cm Article

Metal Methanesulfonates with Mixed Anionic Groups with Large Band Gaps and Enhanced Birefringence

Published as part of Chemistry of Materials virtual special issue "C. N. R. Rao at 90."

Mingli Liang, Yujie Zhang, Eugene Izvarin, Michael J. Waters, James M. Rondinelli, and P. Shiv Halasyamani*

Cite This: https://doi.org/10.1021/acs.chemmater.3c03278 Read Online

ACCESS | Metrics & More | Article Recommendations | Supporting Information

ABSTRACT: Four new metal methanesulfonates with mixed anionic groups, $Bi(SeO_3)(CH_3SO_3)$ (**1**), $Bi(TeO_3)(CH_3SO_3)$ (**2**), $Ba(BF_4)(CH_3SO_3)$ (**3**), and $Ba_2(BF_4)(CH_3SO_3)_3(H_2O)_3$ (**4**), have been successfully synthesized. Compounds **1** and **2** are isomorphic and exhibit a two-dimensional (2D) layered structure. Stereoactive lone pairs are observed with Se^{4+}, Te^{4+}, and Bi^{3+}. Compound **3** features a three-dimensional (3D) structure formed by connecting $[Ba(CH_3SO_3)]^+$ layers via BF_4 tetrahedra, whereas compound **4** features a 2D layered structure, where the BF_4 tetrahedra are positioned on both sides of the $[Ba_2(CH_3SO_3)_3]^+$ layers. The ultraviolet−visible−near-infrared (UV−vis-NIR) spectra indicate that compounds **1** and **2** have absorption edges at 270 and 274 nm, whereas compounds **3** and **4**, with absorption edges below 200 nm, are characterized as deep-UV crystals. Calculations were performed to determine the absorption edges, and comparative analysis indicates a significant enhancement in the calculated birefringence values compared to analogous compounds.

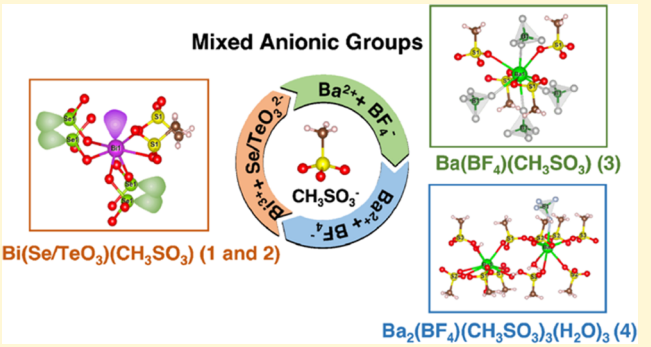

1. INTRODUCTION

In the past decade, there has been a growing interest in solids containing mixed anions or anionic groups.[1−4] Anions of interest include halides, F, Cl, Br, and I,[5−8] and chalcogenides, S, Se, and Te.[2,9−11] The anionic groups can be categorized as follows: (i) π-conjugated oxyanions (e.g., BO_3^{3-}, CO_3^{2-}, NO_3^-);[12−15] (ii) non-π-conjugated oxyanions (e.g., BO_4^{5-}, BF_4^-, PO_4^{3-}, SO_4^{2-});[8,16−18] and (iii) lone-pair active oxyanions (e.g., IO_3^-, SeO_3^{2-}, TeO_3^{2-}, TeO_4^{4-}).[19−22] Some nonlinear optical (NLO) and birefringent materials have notably benefited from this approach.[3,23−31] For instance, in $Ba_4B_{11}O_{20}F$, the combination of F^-, BO_3^{3-}, and BO_4^{5-} results in a stronger second-harmonic generation (SHG) coefficient (10× KDP) and a blue-shifted deep-ultraviolet (DUV) absorption edge (≤175 nm) compared with β-BaB_2O_4 (BBO).[7] In $Pb_2(BO_3)(NO_3)$, the synergy between Pb^{2+}, BO_3^{3-}, and NO_3^- results in a substantial SHG coefficient (9× KDP).[24] Moreover, by introducing IO_3^- into $Pb_3(PO_4)_2$, the birefringence of the resulting compound $Pb_2(IO_3)(PO_4)$ increases from 0.015@1064 nm to 0.060@1064 nm.[25] Notably, the birefringence of $Hg_3(Te_3O_8)(SO_4)$ reaches an impressive 0.166@1064 nm, surpassing the value of 0.093@1064 nm for $HgSO_4$, with TeO_3^{2-} and TeO_4^{4-} playing a crucial role in this enhancement.[28,29]

More recently, metal methanesulfonates ($M(CH_3SO_3)x\cdot nH_2O$) have emerged in the optical crystal field owing to the discovery of $Ba(CH_3SO_3)_2$ as a potential DUV NLO material (1.5× KDP, absorption edge <159 nm).[32] In contrast to SO_4^{2-}, the $CH_3SO_3^-$ anion exhibits the advantages of larger polarizability and a larger HOMO−LUMO gap.[32] Metal methanesulfonates initially attracted attention for their catalytic properties in various organic synthesis reactions.[33,34] A number of the compounds have been reported, encompassing diverse metals (M), including alkali metals (M = Li, Na, K, Rb, Cs),[33,35] alkaline-earth metals (M = Mg, Ca, Sr, Ba),[36,37] transition metals (M = Mn, Cu, Zn, Ag, Cd etc.),[35,37] and post-transition metals (M = Ge, Sn, Pb, Hg).[38−40] There are only three reported bimetallic methanesulfonates, $MAu(CH_3SO_3)_4$ (M = Li, Na, Rb).[41] To the best of our knowledge, metal methanesulfonates with mixed anions or anionic groups have not been reported.

Received: December 22, 2023
Revised: January 31, 2024
Accepted: January 31, 2024

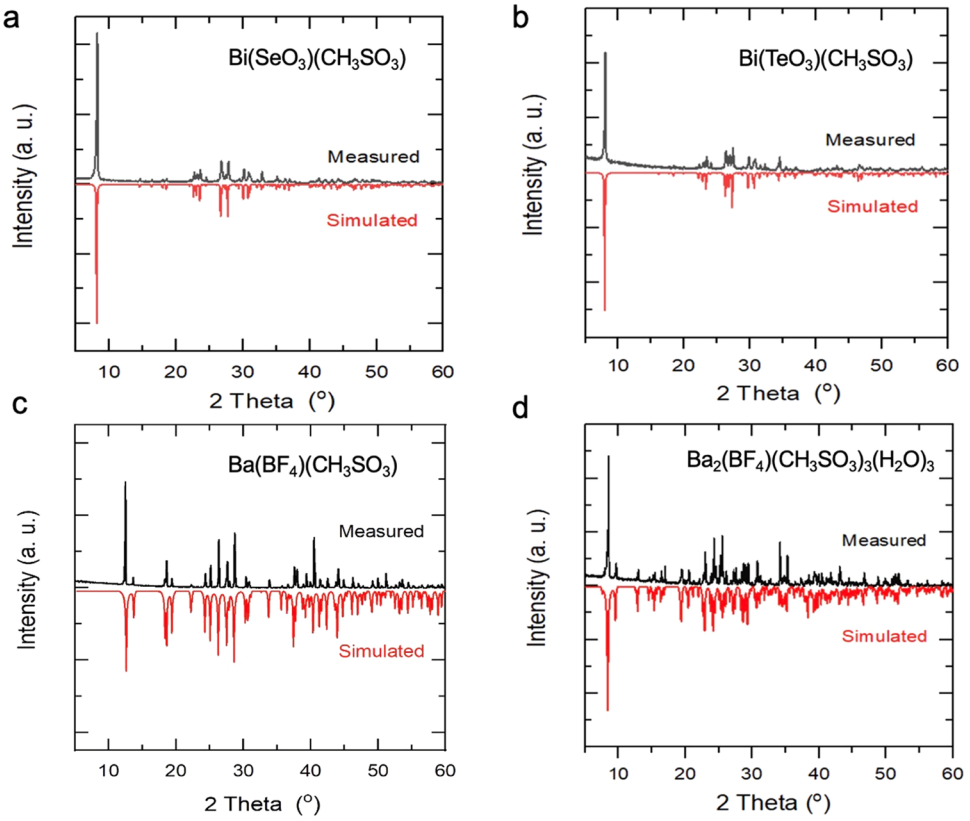

Figure 1. Simulated (red) and measured (black) powder XRD patterns of compounds **1**−**4** (a−d), respectively.

Table 1. Summary of Crystal Data and Structural Refinements for Compounds 1−4

formula	$Bi(SeO_3)(CH_3SO_3)$ (**1**)	$Bi(TeO_3)(CH_3SO_3)$ (**2**)	$Ba(BF_4)(CH_3SO_3)$ (**3**)	$Ba_2(BF_4)(CH_3SO_3)_3(H_2O)_3$ (**4**)
formula weight	431.03	479.67	319.24	700.82
crystal system	monoclinic	monoclinic	orthorhombic	monoclinic
space group	$P2_1/c$	$P2_1/c$	*Pnma*	$P2_1/n$
a/Å	10.9545(16)	11.1536(3)	14.3739(6)	10.9972(11)
b/Å	7.3400(11)	7.4390(2)	6.5475(3)	7.3678(8)
c/Å	8.0937(12)	8.1196(2)	7.4167(3)	23.631(2)
β/°	93.283(2)	94.195(2)	90	99.4740(10)
V/Å^3	649.71(17)	671.89(3)	698.01(5)	1888.6(3)
Z	4	4	4	4
D_{calc}/g·cm^{-3}	4.407	4.742	3.038	2.465
μ/mm^{-1}	13.851	30.779	6.020	4.563
GOF on F^2	1.043	1.039	1.180	1.032
R_1, wR_2 $[I > 2\sigma(I)]$[a]	0.0354, 0.0817	0.0291, 0.0680	0.0132, 0.0330	0.0191, 0.0437
R_1, wR_2 (all data)[a]	0.0447, 0.0872	0.0399, 0.0727	0.0134, 0.0333	0.0209, 0.0445

[a] $R_1 = \sum||F_0| - |F_c||/\sum|F_0|$; $wR_2 = \{\sum w[(F_0)^2 - (F_c)^2]^2/\sum w[(F_0)^2]^2\}^{1/2}$

We present the first report of four metal methanesulfonates incorporating mixed anionic groups, namely, $Bi(SeO_3)(CH_3SO_3)$ (**1**), $Bi(TeO_3)(CH_3SO_3)$ (**2**), $Ba(BF_4)(CH_3SO_3)$ (**3**), and $Ba_2(BF_4)(CH_3SO_3)_3(H_2O)_3$ (**4**). Detailed structural descriptions and physical property characterizations, including thermogravimetry/differential thermogravimetric analysis (TG/DTG), ultraviolet−visible−near-infrared (UV−vis-NIR), and Fourier transform infrared (FT-IR) absorptions are presented. The UV−vis-NIR spectra reveal that the absorption edges of compounds **1** and **2** are at 270 and 274 nm, with those of **3** and **4** falling below 200 nm (DUV region). First-principles calculations provided the following band gap and birefringence values for compounds **1**−**4**, respectively: 4.11, 3.82, 6.43, 5.72 eV, and 0.162, 0.155, 0.034, 0.014 @546 nm. Polarizing microscope measurements yielded comparable measured birefringence values of 0.160, 0.145, 0.034, and 0.013 @546 nm, respectively.

2. EXPERIMENTAL METHODS

2.1. Reagents. All of the chemicals were purchased from Thermo Fisher Scientific Company and used as received: methanesulfonic acid solution (CH_3SO_3H, 70 wt % in water), bismuth nitrate pentahydrate ($Bi(NO_3)_3{\cdot}5H_2O$, 98%+), barium nitrate ($Ba(NO_3)_2$, 99%+), selenium dioxide (SeO_2, 99%+), tellurium dioxide (TeO_2, 99%+), and ammonium tetrafluoroborate (NH_4BF_4, 97%+).

2.2. Syntheses. *2.2.1. Preparations of Compounds 1−3.* Crystals of compounds **1**−**3** were obtained by hydrothermal reactions.

https://doi.org/10.1021/acs.chemmater.3c03278
Chem. Mater. XXXX, XXX, XXX−XXX

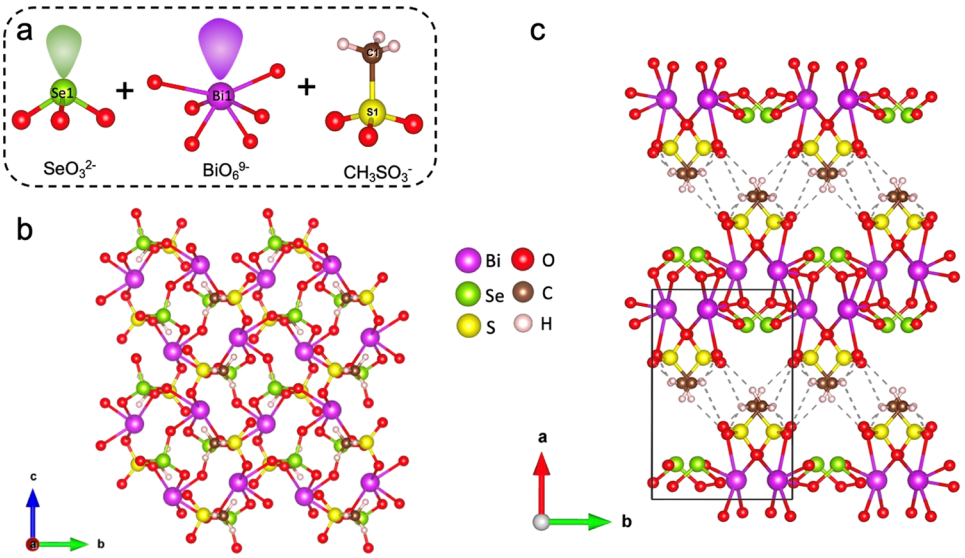

Figure 2. Structure of compound **1**: SeO_3^{2-}, BiO_6^{9-} with stereoactive lone pairs and $CH_3SO_3^-$ ion (a); the 2D $[Bi(SeO_3)(CH_3SO_3)]^0$ layer (b); the view of the structure of compound **1** along the *c*-axis (c).

The reaction components are as follows: $Bi(NO_3)_3{\cdot}5H_2O$ (1.0 mmol, 485.0 mg), CH_3SO_3H (3.6 mmol, 0.5 mL solution), SeO_2 (1.0 mmol, 110.9 mg) for compound **1**; $Bi(NO_3)_3{\cdot}5H_2O$ (1.0 mmol, 485.0 mg), CH_3SO_3H (3.6 mmol, 0.5 mL solution), TeO_2 (1.0 mmol, 159.6 mg) for compound **2**; and $Ba(NO_3)$ (1.0 mmol, 261.4 mg), CH_3SO_3H (3.6 mmol, 0.5 mL solution), NH_4BF_4 (1.3 mmol, 136.3 mg) for compound **3**. The mixtures were placed into Teflon-lined 23 mL autoclaves with 2 mL of deionized water. The autoclaves were closed, heated at 220 °C for 4 days, and slowly cooled to 25 °C at a rate of 6 °C/h. The colorless plate-shaped crystals of compounds **1**−**2** and block-shaped crystals of compound **3** were collected after suction filtration and drying. The yields are about 70% (based on SeO_2), 75% (based on TeO_2), and 55% (based on $Ba(NO_3)_2$) for compounds **1**−**3**, respectively.

2.2.2. Preparation of Compound 4. Crystals of compound **4** were obtained by the solvent evaporation method. $Ba(NO_3)_2$ (4.0 mmol, 1045.6 mg), CH_3SO_3H (36.0 mmol, 5.0 mL solution), NH_4BF_4 (4.0 mmol, 419.4 mg), and 20 mL of deionized water were added to a 50 mL glass beaker. A completely clear solvent was obtained after stirring and filtration. Then, it was placed in a fume hood at room temperature. After evaporation, colorless tabular-shaped crystals of compound **4** were observed. After suction filtration and drying, the average yield of it is about 45% (based on $Ba(NO_3)_2$).

2.3. Powder X-ray Diffraction (XRD). Powder XRD patterns were recorded on a PANalytical Empyrean diffractometer with graphite-monochromated Cu Kα radiation in the 2θ range of 5−60° at room temperature. The purities of the four compounds were confirmed by powder XRD studies (Figure 1).

2.4. Single-Crystal Structure Determination. Single-crystal XRD data for compounds **1**−**4** were collected on a Bruker SMART APEX2 diffractometer equipped with a CCD detector (graphite-monochromated Mo Kα radiation, λ = 0.71073 Å) at room temperature. The SAINT program was applied for data reduction and integration. The structure was determined by the direct methods refined by full-matrix least-squares fitting on F^2 using Olex2−1.5.[42,43] All of the atoms were refined with anisotropic thermal parameters. The structure was checked for missing symmetry elements using PLATON. Crystallographic data and structural refinements of compounds **1**−**4** are listed in Table 1. The atomic coordinates, selected bond distances, and angles are listed in Tables S1−S3.

2.5. Thermal Analysis. Thermogravimetric (TG) analyses were performed with an EXSTAR 6300 TG/DTA Instrument under an N_2 atmosphere between 30−800 °C at a heating rate of 10 °C/min.

2.6. Optical Measurements. Fourier transform infrared (FT-IR) spectra were recorded on a Thermo Fisher Scientific FT-IR spectrometer ranging from 4000 to 400 cm^{-1}. Ultraviolet−visible−near-infrared (UV−vis-NIR) reflectance spectra in the range of 200−2500 nm were recorded on an Agilent Technologies Cary Series 5000 UV−vis-NIR spectrophotometer. The birefringence values of the title compounds were measured by a Nikon Polarizing Microscope (ECLIPSE LV100POL), employing a light source wavelength of 546 nm.

2.7. Theoretical Calculations. All first-principles calculations were performed using the GPAW package (version 23.9.1b1−3d370feb56) with the Atomic Simulation Environment (ASE) (version 3.23.0b1−8f8ba83bc8) for calculation preparation and analysis.[44−46] Ground-state electronic structure calculations were performed with density functional theory (DFT) using the Perdew−Burke−Ernzerhof (PBE) functional. The experimentally determined crystal structures were used for all calculations except for compound **3**, which shows partial occupancy of the hydrogen atoms associated with methyl rotation in the methanesulfonate groups. To avoid the complex treatment of partial occupancies, the partially occupied hydrogen sites were consolidated, and the hydrogen atoms were relaxed under the constraint of maintaining the initial space group symmetry while all other atoms were fixed to their experimentally determined positions. The relaxation was terminated once no atomic force exceeded 5 meV/Å. Self-consistent (SCF) DFT calculations (including the relaxation of compound **3**) were performed with a planewave cutoff of 600 eV, an electronic convergence criterion of 10^{-7} eV for energy eigenvalues, and an electron density convergence criterion of 10^{-5}. Non-self-consistent (NSCF) DFT calculations were performed with extra bands, ensuring 40 eV empty bands above the conduction band were converged and finer *k*-point grids than SCF calculations in preparation for optical calculations. All *k*-points grids were Γ-centered; for SCF calculations, compounds **1**, **2**, **3**, and **4** were studied with grids of (4 × 4 × 4), (4 × 4 × 4), (2 × 4 × 4), and (4 × 4 × 2) and for NSCF calculations grids of (8 × 8 × 8), (8 × 8 × 8), (4 × 8 × 8), and (4 × 8 × 2) were used, respectively. Linear optical properties were computed by the sum-over bands approach up to photon energies of 40 eV, with 20 meV broadening. No scissor shifts were applied since DFT band gaps were found to closely match the experimental band gaps. Electronic band structures were computed using 128 *k*-points along the high symmetry *k*-paths in the Brillouin zones specified by the AFLOW standard.[47]

The response electron distribution anisotropy (REDA) method was employed to investigate the origin of birefringence (Δn).[48,49] In this method, birefringence is directly proportional to the REDA index and can be expressed by the following equation

https://doi.org/10.1021/acs.chemmater.3c03278
Chem. Mater. XXXX, XXX, XXX−XXX

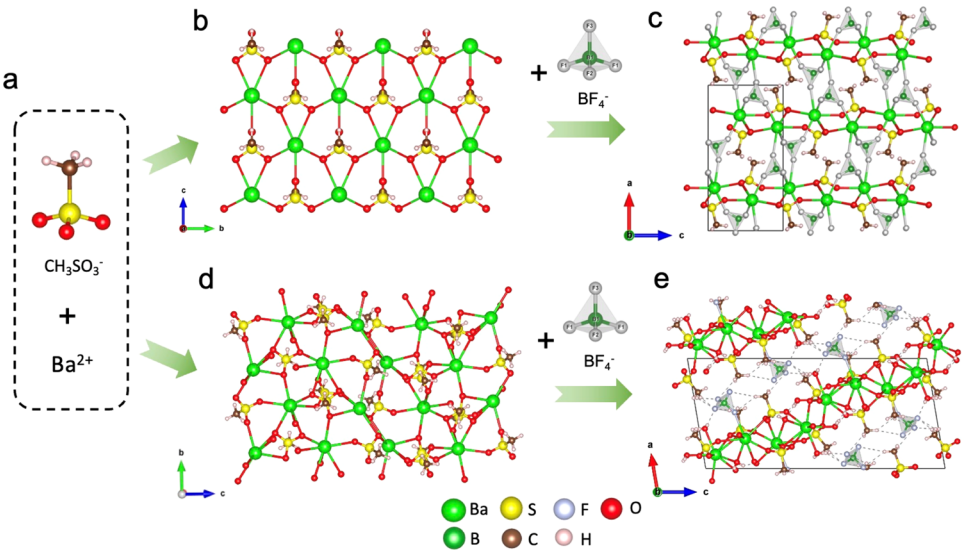

Figure 3. Structure of compounds **3** and **4**: Ba^{2+} and $CH_3SO_3^-$ ions (a); the 2D layers of $[Ba(CH_3SO_3)]^+$ and $[Ba_2(CH_3SO_3)_3]^+$, respectively (b, d); the view of the structures of compounds **3** and **4** along the *b*-axis (c, e).

$$\Delta n = \frac{R\sum_g [N_c Z_a \Delta\rho^b]_g}{2n_1 E_o}$$

Here, R represents the correction coefficient; N_c indicates the coordination number of adjacent cations to the central anion; Z_a represents the formal chemical valence of the anion; E_o denotes the optical band gap; $\Delta\rho^b$ is the difference between the maximum and minimum of the covalent electron density of the covalent bond on the optical principal axes; and n_1 is the minimum refractive index.

3. RESULTS AND DISCUSSION

3.1. Crystal Structure. *3.1.1. Structures of Compounds 1 and 2.* Compounds **1** and **2** are isostructural and crystallize in the centrosymmetric space group $P2_1/c$ (No. 14). They feature a 2D layered structure consisting of Bi^{3+}, SeO_3^{2-}(**1**)/TeO_3^{2-}(**2**), and $CH_3SO_3^-$ ions. For illustrative purposes, compound **1** has been chosen to represent the structural characteristics (Figure 2). The asymmetric unit contains one Bi, one Se, one S, six O, one C, and three H atoms (Table S1). Bi(1) exhibits a 6-fold coordination, with the Bi−O bond distances ranging from 2.188(7)−2.755(7) Å (Table S2). Within the distorted BiO_6 polyhedron, a stereoactive lone pair is present (Figure 2a). Se(1) is coordinated to three O atoms, forming a distorted $Se(1)O_3$ trigonal pyramid, also with a stereoactive lone pair (Figure 2a). The Se−O bond distances range from 1.701(7)−1.733(7) Å (Table S2), and the O−Se−O bond angles range from 97.0(3)−103.8(3)° (Table S3). S(1) coordinates with three O atoms and one methyl group (−CH_3), forming a $CH_3SO_3^-$ anion. It can be considered as a CH_3SO_3 distorted tetrahedron with the S−O bond distances spanning from 1.431(7)−1.478(7) Å and an S−C bond distance of 1.732(11) Å (Table S2). The O−S−O and O−S−C bond angles range from 106.5(4)−113.6(5) and 105.6(5)−109.1(5)°, respectively (Table S3). The bond distances and angles are consistent with those reported earlier.[19,41,50−52] In the structure, the BiO_6 polyhedron is connected to four SeO_3 trigonal pyramids and two CH_3SO_3 tetrahedra by corner-shared interactions, forming a 2D $[Bi(SeO_3)(CH_3SO_3)]^0$ layer within the *bc*-plane (Figure 2b). The C−H···O hydrogen bonds (3.396(14) Å, 161(5)°) become the main attractive force between the 2D layers (Table S4 and Figure 2c). In connectivity terms, the structure may be written as $\{[BiO_{4/2}O_{2/3}]^{7/3-}\ [SeO_{2/2}O_{1/3}]^{4/3+}\ [CH_3SO_{2/2}O_{1/1}]^+\}^0$. Bond valence sum (BVS) calculations for compounds **1** and **2** yield values of 2.78/2.89, 3.90, 3.84, 5.96, 1.65−2.10, and 4.27/4.21 for Bi, Se, Te, S, O, and C atoms, respectively, consistent with their oxidation states of +3, +4, +4, +6, −2, −4 (Table S1).[53]

3.1.2. Structures of Compounds 3 and 4. Compounds **3** and **4** both consist of Ba^{2+}, BF_4^- and $CH_3SO_3^-$ ions. They crystallize in different centrosymmetric space groups, *Pnma* (No.62) for compound **3** and $P2_1/n$ (No.14) for compound **4**. Their structures are shown in Figure 3. With compound **3**, the asymmetric unit contains one Ba, one S, three F, two O, one C, one B, and three H atoms (Table S1). Ba(1) exhibits a nine-coordinated environment with four F and five O atoms with Ba−F (Ba−O) bond distances ranging from 2.6422(19)−2.8103(17) Å (2.721(2)−2.9493(3) Å) (Table S2). S(1) and C(1) belong to a $CH_3SO_3^-$ anion and form a distorted tetrahedron. The S−O bond distances range between 1.448(2) and 1.4632(15) Å, and the S−C bond distance is 1.759(3) Å (Table S2). The O−S−O and O−S−C bond angles range from 109.68(12)−112.21(8) and 106.85(14)−107.83(9)°, respectively (Table S3). B(1) is coordinated with four F atoms, forming a BF_4 tetrahedron with the B−F bond distances ranging from 1.367(2)−1.397 Å and F−B−F bond angles ranging from 107.7(3)−110.82(16)° (Tables S2 and S3). The bond distances and angles are consistent with the previously reported values.[41,54−56] In the structure, Ba^{2+} connected with four CH_3SO_3 distorted tetrahedra by corner-shared or edge-shared interactions, forming a 2D $[Ba(CH_3SO_3)]^+$ layer within the *bc*-plane (Figure 3a,3b). These layers are further connected by BF_4 polyhedra into a 3D structure (Figure 3c). In connectivity terms, the structure may be described as $\{[BaO_{4/3}O_{1/2}F_{4/2}]^{11/3-}\ [BF_{4/2}]^+\ [CH_3SO_{2/3}O_{1/2}]^{8/3+}\}^0$. BVS calculations on compound **3** result in values of 2.04, 5.88, 1.00−1.11, 1.92/2.08, 4.18, and 3.32 for Ba, S, F, O, C, and B atoms, consistent with their oxidation states of +2, +6, −1, −2, −4, and +3, respectively (Table S1).[53]

For compound **4**, the asymmetric unit encompasses two Ba, three S, four F, 12 O, three C, one B, and 15 H atoms (Table S1). Ba(1) is nine-coordinated with nine O atoms, and the Ba−O bond distances range from 2.776(2) to 3.175(2) Å

https://doi.org/10.1021/acs.chemmater.3c03278
Chem. Mater. XXXX, XXX, XXX−XXX

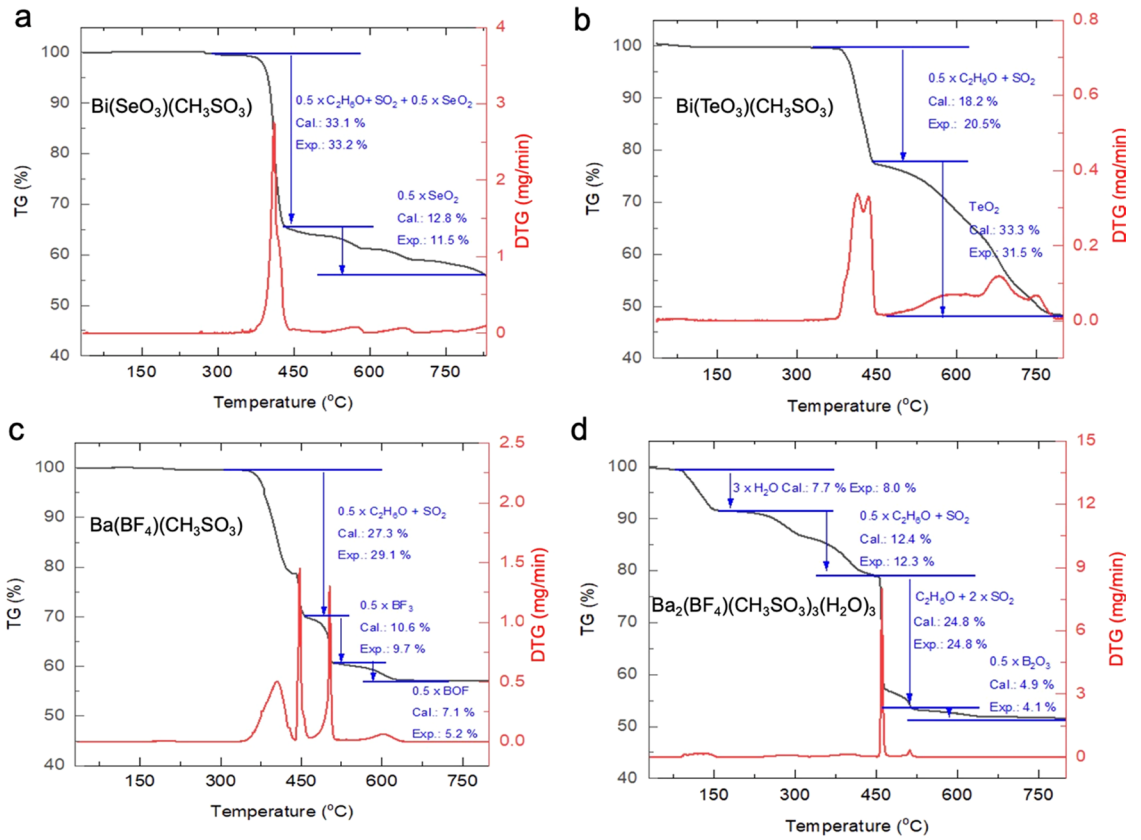

Figure 4. TG and DTG curves of the compounds **1**–**4**, with calculated (Cal.) and experimental (Exp.) values provided.

(Table S2). Ba(2) is eight-coordinated with seven O atoms and one F atom, where Ba–O bond distances fall within the range of 2.7249(19)–2.9366(19) Å, and the Ba–F bond distance is 2.803(2) Å (Table S2). Each of the three S atoms is connected to three O atoms and one $-CH_3$ group to form a CH_3SO_3 distorted tetrahedron. The S–O bond distances range from 1.443(2)–1.4603(19) Å, and the S–C bond distances range from 1.747(3)–1.749(3) Å (Table S2). The O–S–O bond angles range from 109.54(11)–114.29(13)°, and the O–S–C bond angles range from 106.24(15)–108.04(15)° (Table S3). B(1) is connected with four F atoms to form a BF_4 octahedron with the B–F bond distances range from 1.330(5)–1.413(4) Å (Table S2) and the F–B–F bond angles range from 107.8(3)–112.1(3)° (Table S3). The bond distances and angles are consistent with the previously reported values.[41,54−57] Within the structure, $Ba(1)^{2+}$ and $Ba(2)^{2+}$ are linked with CH_3SO_3 distorted tetrahedra by corner-shared or edge-shared interactions, resulting in the formation of a 2D $[Ba_2(CH_3SO_3)_3]^+$ layer (Figure 3d). The BF_4 octahedra and H_2O molecules are suspended on the upper and lower sides of this layer. These layers are mainly held together by C–H···F hydrogen bonds (3.442(4) Å, 160(5)°) (Figure 3e and Table S4). In connectivity terms, the structure may be described as $\{[BaO_{4/3}O_{2/2}]^{8/3-}\ [BaO_{4/3}O_{3/2}F_{1/2}]^{25/6-}\ [BF_{1/2}F_{3/1}]^{1/2-}\ [CH_3SO_{2/2}O_{1/3}]^{7/3+}\ [CH_3SO_{3/3}]^{3+}\ [CH_3SO_{3/2}]^{2+}\ 3[H_2O]\}^0$. BVS calculations on compound **4** gave values of 2.08/2.10, 5.94–5.98, 0.88–0.95, 1.76–2.06, 4.21–4.22, and 3.44 for Ba, S, F, O, C, and B atoms, consistent with oxidation states of +2, +6, −1, −2, −4, and +3, respectively (Table S1).[53]

3.2. Thermal Analysis. TG analysis studies indicate that compounds **1**–**4** exhibit stability up to temperatures of approximately 380, 380, 345, and 90 °C, respectively (Figure 4). Compounds **1** and **2** display two main stages of weight loss. For compound **1** (Figure 4a), the first stage corresponds to the decomposition of $CH_3SO_3^-$ and a portion of SeO_3^{2-} anions. $CH_3SO_3^-$ decomposes into 0.5 molecule organic carbon oxides (C_2H_6O) and 1.0 molecule SO_2 gas,[58] while SeO_3^{2-} releases 0.5 molecule of SeO_2 (Cal.: 33.1%, Exp.: 33.2%).[19] The subsequent stage involves the gradual release of the remaining 0.5 molecule of SeO_2 (Cal.: 12.8%, Exp.: 11.5%). Concerning compound **2** (Figure 4b), the decompositions of $CH_3SO_3^-$ and TeO_3^{2-} anions are separated due to the higher decomposition temperature of TeO_3^{2-}.[59] Its initial stage entails the release of 0.5 molecule of C_2H_6O and 1.0 molecule of SO_2 (Cal.: 18.2%, Exp.: 20.5%), followed by a second stage involving the release of 1.0 molecule of TeO_2 (Cal.: 33.3%, Exp.: 31.5%). Powder XRD analysis reveals that the ultimate residue for compounds **1** and **2** at 800 °C is Bi_2O_3 (Cal.: 54.1%, Exp.: 55.3% for compound **1**; Cal.: 48.5%, Exp.: 48.0% for compound **2**) (Figure S1a).

As for compound **3**, the weight loss process unfolds in four stages (Figure 4c). The initial two stages correspond to the decomposition of $CH_3SO_3^-$ anion, releasing 0.5 molecule of C_2H_6O and 1.0 molecule of SO_2 (Cal.: 27.3%, Exp.: 29.1%). The third stage involves the elimination of 0.5 molecule of BF_3 (Cal.: 27.3%, Exp.: 29.1%). The remaining boron element is liberated in the fourth step in the form of 0.5 molecule of BOF (Cal.: 7.1%, Exp.: 5.2%). Moving to compound **4**, its weight loss process encompasses five stages (Figure 4c). The first stage corresponds to the removal of 3.0 molecules of H_2O (Cal.: 7.7%, Exp.: 8.0%). The second and third stages involve the decomposition of $CH_3SO_3^-$ anion, gradually releasing 0.5 molecule of C_2H_6O and 1.0 molecule of SO_2 (Cal.: 12.4%,

https://doi.org/10.1021/acs.chemmater.3c03278
Chem. Mater. XXXX, XXX, XXX−XXX

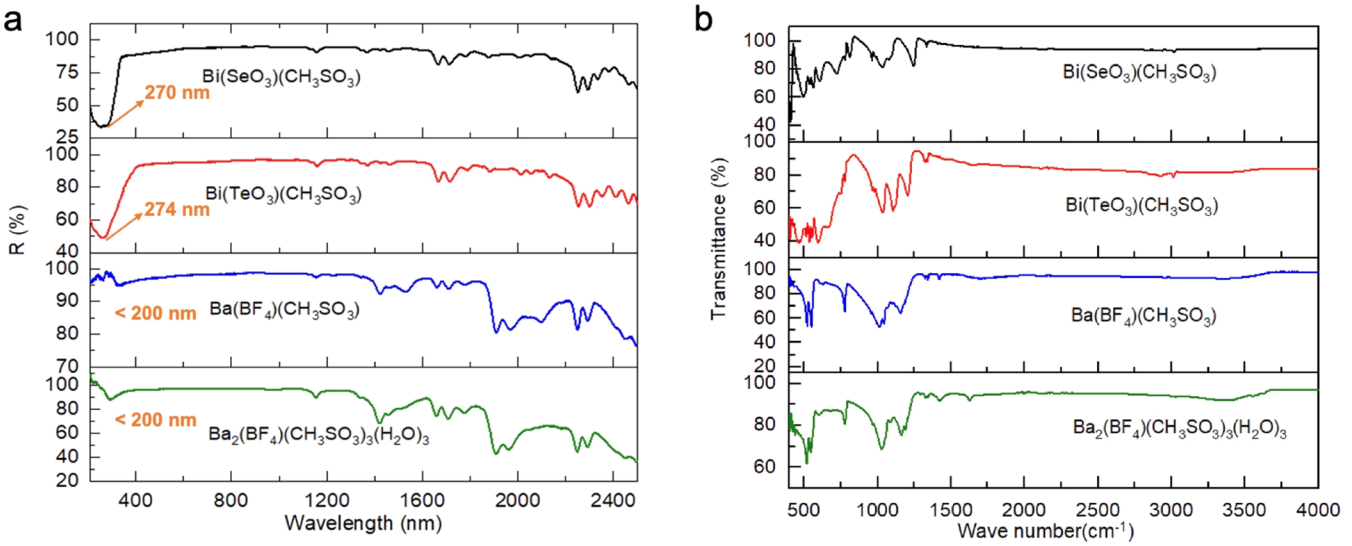

Figure 5. UV−vis-NIR reflectance spectra (a) and the FT-IR spectra (b) of compounds **1**−**4**.

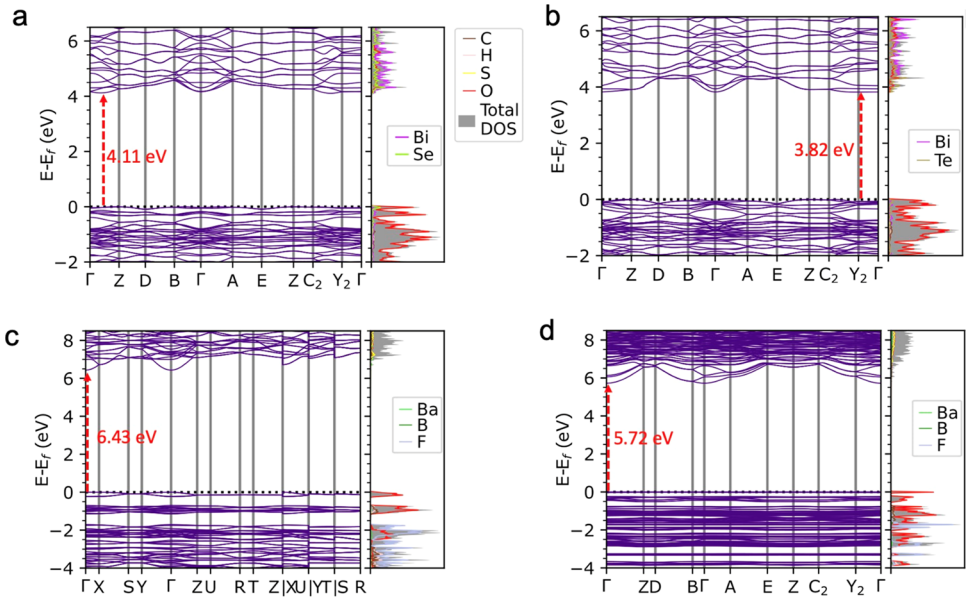

Figure 6. Electronic band structures and PDOS of compounds **1**−**4** (a−d).

Exp.: 12.3%). Once the temperature reaches 450 °C (the fourth stage), the remaining $CH_3SO_3^-$ anion rapidly decomposes, releasing 1.0 molecule of C_2H_6O and 2.0 molecules of SO_2 (Cal.: 24.8%, Exp.: 24.8%). The fifth stage corresponds to the loss of 0.5 molecule of B_2O_3 (Cal.: 4.9%, Exp.: 4.1%). The ultimate residue of compounds **3** and **4** at 800 °C is BaF_2 (Cal.: 55.0%, Exp.: 56.0% for compound **3**; Cal.: 50.0%, Exp.: 50.8% for compound **4**) (Figure S1b).

3.3. Optical Properties. UV−vis-NIR reflectance spectra analyses were conducted in the wavelength range of 200−2500 nm for compounds **1**−**4** (Figure 5a). The results indicate that the absorption cutoff edges for compounds **1**−**2** fall within the UV region, with maximum absorption wavelengths at 270 nm for compound **1** and 274 nm for compound **2**. The optical band gap (E_0) values were determined as 3.90 and 3.67 eV, respectively (Figure S2). For compounds **3** and **4**, their absorption cutoff edges extend into the DUV region (<200 nm). Unfortunately, we could not determine the E_0 values for them due to limitations in our measurement instrument (≥200 nm). Instead, their band gaps were given by subsequent DFT calculations.

The FT-IR spectra of compounds **1**−**4** have been measured in the wavenumber range of 4000−400 cm^{-1} at room temperature (Figure 5b). The C−H bond vibrations appeared between 1300 and 1500 cm^{-1}, and the peaks from 800 to 1300 cm^{-1} can be ascribed to S−O and S−C bond vibrations.[35,60] In the case of compounds **1** and **2**, the Se−O and Te−O bond vibrations are observed within the range of 500−800 cm^{-1}.[61] And the peaks observed between 400 and 500 cm^{-1} can be attributed to Se−O−Bi and Te−O−Bi vibrations. In compounds **3** and **4**, the characteristic vibrations of BF_4 are present at around 770, 510, and 543 cm^{-1}.[62,63] The peak at 1634 cm^{-1} and broad peak at around 3300 cm^{-1} of compound **4** suggest the presence of O−H bending and stretching, respectively.[61]

3.4. Theoretical Calculations. Theoretical calculations were performed using the experimentally determined crystal structures except for compound **3**, where methyl rotation yield

https://doi.org/10.1021/acs.chemmater.3c03278
Chem. Mater. XXXX, XXX, XXX−XXX

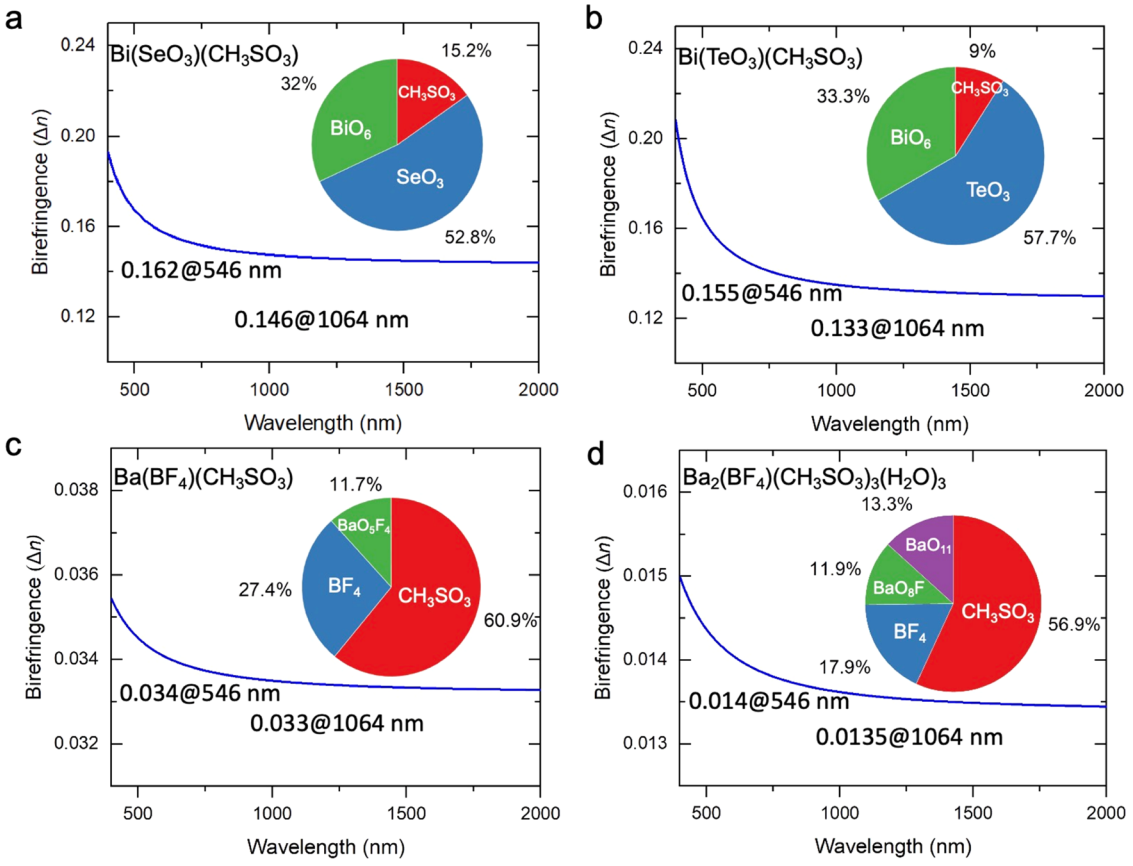

Figure 7. Calculated birefringence (Δn) of compounds **1**−**4** (a−d); inset, pie charts: the birefringence contribution percentages of different units were calculated by the REDA method.

degenerate hydrogen partial site occupation. To simplify calculations, the hydrogen atom positions were relaxed while constrained to the experimentally determined space group symmetry. All other atoms were fixed in their experimentally determined positions. After relaxation, the C−H bond lengths are 1.095 Å, the S−C−H bond angles are 109°, and the S−O−C−H dihedral angles are 60°.

Electronic band structures and projected densities of states (PDOS) were computed at the DFT level and are shown in Figure 6. The DFT band gaps for compounds **1**, **2**, **3**, and **4** are all indirect and are 4.11, 3.82, 6.43, and 5.72 eV, respectively. For compounds **1** and **2**, where optical measurements of the band gaps were possible, DFT, unusually, overpredicts the band gaps. While subgap optical phenomena, such as excitons, could explain the usually good agreement, no experimental evidence of them was observed. All compounds exhibit valence bands composed mostly of O 2p-states with low dispersion, which is expected with molecular solids with large unit cells. The conduction band minima are located between Γ-*Z*, at *Y*, at Γ, and at Γ for compounds **1**, **2**, **3**, and **4**, respectively (Figure 6). Being isoelectronic and isostructural, compounds **1** and **2** have similar electronic structures where Bi/Se and Bi/Te p-states comprise the conduction bands (Figure 6a,b). In compounds **3** and **4**, the lowest conduction bands are from the Ba 6s-states. Above those, the conduction bands are loosely localized on a mixture of S and O p-states (Figure 6c,d). Notably, in compound **4**, the incorporation of H_2O introduces a narrow band of O 2p-states above the existing band edge. The lack of band dispersion of these states indicates they are the isolated molecular states corresponding to the H_2O HOMO states. Likewise, the conduction band states introduced below Ba 6*s*-states are likely the H_2O LUMO states, given that a DFT study of ice found a band gap of 5.55 eV,[64] which closely matches the 5.72 eV of compound **4**. Therefore, the influence of H_2O molecules on its electronic structure is a key factor contributing to the reduced band gap compared to compound **3**.

Linear optical property calculations were performed for all compounds yielding frequency-dependent complex refractive index spectra, which are provided in the Supporting Information (Figures S3−S6). Figure 7 shows the calculated birefringence of the compounds **1**−**4** within the range of 400−2000 nm. The birefringence values of compounds **1** and **2** are significant, calculated as 0.162 and 0.155 @546 nm (0.146 and 0.133 @1064 nm), respectively, while the birefringence values of compounds **3** and **4** are small, calculated as 0.034 and 0.014 @546 nm (0.033 and 0.0135 @1064 nm), respectively. A polarizing microscope, employing a light source wavelength of 546 nm, has been used to measure the birefringence of the four compounds. The measured birefringence values are as follows: 0.160, 0.145, 0.034, and 0.013 @546 nm, respectively (Figure S7). The calculated values are slightly higher than the measured values because local field effects were not included.

To gain a deeper insight into the impact of the $CH_3SO_3^-$ anion on band gaps and birefringence, a further comparison of these properties among reported bismuth selenites/tellurites and barium tetrafluoroborates is presented in Table 2. For bismuth selenites/tellurites, it is evident that the band gaps of $Bi_2O_2(SeO_3)$, $Bi_2(SeO_3)_3$, and $Bi_2O_2(TeO_3)$ do not surpass 3.50 eV.[40,65] When incorporating other anions such as F^-,

https://doi.org/10.1021/acs.chemmater.3c03278
Chem. Mater. XXXX, XXX, XXX−XXX

Table 2. Band gaps and Birefringence of Bismuth Selenites/Tellurites and Barium Tetrafluoroborates without Additional Transition Metals

compound	space group	E_g (eV)	Δn (@ nm)	refs
Bismuth Selenites				
$Bi_2O_2(SeO_3)$	*Aem*2	3.30[a]	N/A	65
$Bi(SeO_3)(NO_3)$	*C*2/*c*	3.43[b]	N/A	66
$Bi_2(SeO_3)_3$	$P2_1/c$	3.50[a]	N/A	65
$Bi_3O_2(SeO_3)_2(NO_3)$	$P2_1/c$	3.59[b]	N/A	67
$Bi_2K_2(SeO_3)_3F_2$	*Cm*	3.72[b]	0.091@546[b]	68
$Bi_2Rb_2(SeO_3)_3F_2$	*Cm*	3.73[b]	0.08@546[b]	68
$Bi_3(SeO_3)_3(Se_2O_5)F$	$P2_1$	3.80[b]	N/A	69
$Bi_2[B_2(SeO_3)_6]$	$P2_1$/n	3.83[b]	0.09@1064[a]	70
$BiSeO_3F$	$Pca2_1$	3.83[b]	0.144@1064[a]	19
$Bi(SeO_3)(CH_3SO_3)$ (**1**)	$P2_1/c$	3.90[b]	0.162@546[a]	this work
Bismuth Tellurites				
$Bi_2O_2(TeO_3)$	*Abm*2	3.21[b]	N/A	50
$Bi_4TeO_4F_2(TeO_3)_2(SeO_3)_2$	$P2_1/c$	3.24[b]	0.20@1064[a]	71
$Bi_3(OH)(TeO_3)_3(NO_3)_2$	*P*-62*m*	3.31[b]	N/A	66
$Bi_2(TeO_3)_2(SO_4)$	*C*2/*c*	3.60[b]	N/A	72
$Bi(TeO_3)(NO_3)$	$P2_1/c$	3.62[b]	N/A	67
$Bi(TeO_3)(CH_3SO_3)$ (**2**)	$P2_1/c$	3.67[b]	0.155@546[a]	this work
$Bi_3F(TeO_3)(TeO_2F_2)_3$	$P6_3mc$	3.85[b]	N/A	73
Barium Tetrafluoroborates				
$Ba_2(BF_4)(CH_3SO_3)_3(H_2O)_3$ (**4**)	$P2_1/n$	5.72[a]	0.014@546[a]	this work
$Ba(BF_4)Cl$	$Pmn2_1$	6.111[a]	0.014@1064[a]	74
$Ba(BF_4)(AsF_6)$	*Pnma*	6.260[a]	0.002@1064[a]	74
$Ba_2(BF_4)_2(AsF_6)(H_3F_4)$	$P6_3/mmc$	6.309[a]	0.010@1064[a]	74
$Ba(BF_4)(CH_3SO_3)$ (**3**)	*Pnma*	6.43[a]	0.034@546[a]	this work
$Ba(BF_4)(PF_6)$	*P*-62*m*	8.065[a]	0.001@1064[a]	74
$Ba(BF_4)_2$	*C*2/*m*	8.451[a]	0.008@1064[a]	74

[a]Calculated result. [b]Experiment result.

NO_3^-, SO_4^{2-}, BO_4^{5-}, and $CH_3SO_3^-$, the band gaps exhibit varying degrees of enlargement.[19,66−73] In particular, compound **1** boasts the largest band gap at 3.90 eV. And compound **2**, with a band gap of 3.67 eV, only falls short of $Bi_3F(TeO_3)(TeO_2F_2)_3$ (3.85 eV) within the bismuth tellurates.[73] The enhanced band gap of compounds **1** and **2** is primarily attributed to the large HOMO−LUMO gap (8.59 eV) of the $CH_3SO_3^-$ anion.[32] Conversely, for the barium tetrafluoroborates, the introduction of anions such as Cl^-, PF_6^-, AsF_6^-, and $CH_3SO_3^-$ leads to a reduction in band gaps. $Ba(BF_4)_2$ without mixed anions exhibits the largest calculated band gap of 8.451 eV.[74] This is because the BF_4^- anion possesses a very large HOMO−LUMO gap of approximately 9.34 eV.[75] Then, the addition of anions with smaller HOMO−LUMO gaps has the opposite effect.

Moreover, the influence of $CH_3SO_3^-$ anion with large polarizability on birefringence should not be underestimated.[32] Herein, to better elucidate the individual contributions of different units to the birefringence of compounds **1**−**4**, we calculated their bonding electron density differences ($\Delta\rho$) using the REDA method (Table S5 and Figure 7).[48,49] For compounds **1** and **2**, the $[BiO_6]$, $[SeO_3]$ and $[TeO_3]$ units with stereoactive lone pairs are the most significant contributors (>30, 52.8 and 57.7%, respectively), and the $[CH_3SO_3]$ units contribute around 10%. Hence, the substantial birefringence (0.162 and 0.155 @546 nm, respectively) of compounds **1** and **2** can be attributed to the cumulative impact of the different units involved. For compounds **3** and **4**, the contributions of $[CH_3SO_3]$ units markedly increase to 60.9 and 56.9%, respectively, followed by $[BF_4]$ units (27.4 and 17.9%, respectively). $[BaO_5F_4]$, $[BaO_{11}]$, and $[BaO_8F]$ units contribute the least to the birefringence. Although the birefringence of compounds **3** and **4** are small (0.034 and 0.014 @546 nm, respectively), they still represent an increase compared to other barium tetrafluoroborates,[74] which can be attributed to the incorporation of $CH_3SO_3^-$ anion.

4. CONCLUSIONS

In summary, four novel metal methanesulfonates with mixed anionic groups, namely, $Bi(SeO_3)(CH_3SO_3)$ (**1**), $Bi(TeO_3)(CH_3SO_3)$ (**2**), $Ba(BF_4)(CH_3SO_3)$ (**3**), and $Ba_2(BF_4)(CH_3SO_3)_3(H_2O)_3$ (**4**), have been synthesized successfully for the first time. Compounds **1** and **2** are isostructural, exhibiting a 2D layered structure composed of Bi^{3+} action and SeO_3^{2-}/TeO_3^{2-}, $CH_3SO_3^-$ anions. Compounds **3** and **4** display a 3D structure and a 2D layered structure, respectively, composed of Ba^{2+} cation and BF_4^-, $CH_3SO_3^-$ anions. These four compounds demonstrate large band gaps. Compounds **1** and **2** exhibit significant birefringence values of 0.162 and 0.155 @546 nm, respectively, which can be attributed to the combined contributions of $[Se/TeO_3]$, $[BiO_6]$, and $[CH_3SO_3]$ units. And the birefringence values of compounds **3** and **4** (0.034 and 0.014 @546 nm, respectively) are improved compared to other barium tetrafluoroborates, with the $[CH_3SO_3]$ unit being the predominant contributor.

■ ASSOCIATED CONTENT

Supporting Information

The Supporting Information is available free of charge at https://pubs.acs.org/doi/10.1021/acs.chemmater.3c03278.

Crystal data, atomic coordinates, important bond distances and angles, optical band gaps, the full frequency-dependent linear optical properties of the title compounds, measured birefringence, bonding electron difference, and contribution percentages of different units (PDF)

Accession Codes

CCDC 2308320−2308323 contain the supplementary crystallographic data for this paper. These data can be obtained free of charge via www.ccdc.cam.ac.uk/data_request/cif, by emailing data_request@ccdc.cam.ac.uk, or by contacting The Cambridge Crystallographic Data Centre, 12 Union Road, Cambridge CB2 1EZ, U.K.; fax: + 44 1223 336033.

■ AUTHOR INFORMATION

Corresponding Author

P. Shiv Halasyamani − *Department of Chemistry, University of Houston, Houston, Texas 77204, United States;* orcid.org/0000-0003-1787-1040; Email: psh@uh.edu

https://doi.org/10.1021/acs.chemmater.3c03278
Chem. Mater. XXXX, XXX, XXX−XXX

Authors

Mingli Liang − *Department of Chemistry, University of Houston, Houston, Texas 77204, United States*

Yujie Zhang − *Department of Chemistry, University of Houston, Houston, Texas 77204, United States*

Eugene Izvarin − *Department of Chemistry, University of Houston, Houston, Texas 77204, United States*

Michael J. Waters − *Material Science and Engineering, Northwestern University, Evanston, Illinois 60208, United States;* orcid.org/0000-0001-6425-4331

James M. Rondinelli − *Material Science and Engineering, Northwestern University, Evanston, Illinois 60208, United States;* orcid.org/0000-0003-0508-2175

Complete contact information is available at: https://pubs.acs.org/10.1021/acs.chemmater.3c03278

Notes

The authors declare no competing financial interest.

■ ACKNOWLEDGMENTS

M.L., Y.Z., E.I., and P.S.H. thank the Welch Foundation (Grant E-1457) and the NSF (DMR − 2002319) for support. The computational work by M.J.W. and J.M.R. was supported by the National Science Foundation (NSF) Grant No. DMR-2011208 and they used resources of the National Energy Research Scientific Computing Center (NERSC), a U.S. DOE Office of Science User Facility located at Lawrence Berkeley National Laboratory, operated under Contract No. DE-AC02-05CH11231.

■ REFERENCES

(1) Kageyama, H.; Hayashi, K.; Maeda, K.; Attfield, J. P.; Hiroi, Z.; Rondinelli, J. M.; Poeppelmeier, K. R. Expanding Frontiers in Materials Chemistry and Physics with Multiple Anions. *Nat. Commun.* **2018**, *9*, No. 772.

(2) Li, Y. Y.; Wang, W. J.; Wang, H.; Lin, H.; Wu, L. M. Mixed-Anion Inorganic Compounds: A Favorable Candidate for Infrared Nonlinear Optical Materials. *Cryst. Growth Des.* **2019**, *19* (7), 4172−4192.

(3) Pan, Y.; Guo, S. P.; Liu, B. W.; Xue, H. G.; Guo, G. C. Second-Order Nonlinear Optical Crystals with Mixed Anions. *Coord. Chem. Rev.* **2018**, *374*, 464−496.

(4) Shang, M.; Halasyamani, P. S. Mixed Lone-Pair and Mixed Anion Compounds: $Pb_3(SeO_3)(HSeO_3)Br_3$, $Pb_3(SeO_3)(OH)Br_3$, $CdPb_8(SeO_3)_4Cl_4Br_6$ and $RbBi(SeO_3)F_2$. *J. Solid State Chem.* **2020**, *282*, No. 121121.

(5) Schnelle, W.; Schmid, H. Magnetic and Structural Phase Transitions of Multiferroic Boracites $M_3B_7O_{13}X$ (M = 3d Transition Metal Cr-Zn or Mg; X = halogen Cl, Br, I). *Phys. Rev. B* **2015**, *91* (18), No. 184411.

(6) Wu, H.; Pan, S.; Poeppelmeier, K. R.; Li, H.; Jia, D.; Chen, Z.; Fan, X.; Yang, Y.; Rondinelli, J. M.; Luo, H. $K_3B_6O_{10}Cl$: A New Structure Analogous to Perovskite with a Large Second Harmonic Generation Response and Deep UV Absorption Edge. *J. Am. Chem. Soc.* **2011**, *133* (20), 7786−7790.

(7) Wu, H.; Yu, H.; Yang, Z.; Hou, X.; Su, X.; Pan, S.; Poeppelmeier, K. R.; Rondinelli, J. M. Designing a Deep-Ultraviolet Nonlinear Optical Material with a Large Second Harmonic Generation Response. *J. Am. Chem. Soc.* **2013**, *135* (11), 4215−4218.

(8) Yu, P.; Wu, L. M.; Zhou, L. J.; Chen, L. Deep-Ultraviolet Nonlinear Optical Crystals: $Ba_3P_3O_{10}X$ (X = Cl, Br). *J. Am. Chem. Soc.* **2014**, *136* (1), 480−487.

(9) Chung, I.; Song, J.-H.; Jang, J. I.; Freeman, A. J.; Kanatzidis, M. G. $Na_2Ge_2Se_5$: A Highly Nonlinear Optical Material. *J. Solid State Chem.* **2012**, *195*, 161−165.

(10) Tan, D.-M.; Lin, C.-S.; Luo, Z.-Z.; Zhang, H.; Zhang, W.-L.; He, Z.-Z.; Cheng, W.-D. Synthesis and Characterization of a New Mid-Infrared Transparent Compound: Acentric $Ba_5In_4Te_4S_7$. *Dalton Trans.* **2015**, *44* (16), 7673−7678.

(11) Kuo, S.-M.; Chang, Y.-M.; Chung, I.; Jang, J.-I.; Her, B.-H.; Yang, S.-H.; Ketterson, J. B.; Kanatzidis, M. G.; Hsu, K.-F. New Metal Chalcogenides $Ba_4CuGa_5Q_{12}$(Q = S, Se) Displaying Strong Infrared Nonlinear Optical Response. *Chem. Mater.* **2013**, *25* (12), 2427−2433.

(12) Zhang, X.; Wang, L.; Wang, X.; Wang, G.; Zhu, Y.; Chen, C. High-Power Sixth-Harmonic Generation of an Nd:YAG Laser with $KBe_2BO_3F_2$ Prism-Coupled Devices. *Opt. Commun.* **2012**, *285*, 4519−4522.

(13) Peng, G.; Ye, N.; Lin, Z.; Kang, L.; Pan, S.; Zhang, M.; Lin, C.; Long, X.; Luo, M.; Chen, Y.; Tang, Y.-H.; Xu, F.; Yan, T. $NH_4Be_2BO_3F_2$ and γ-Be_2BO_3F: Overcoming the Layering Habit in $KBe_2BO_3F_2$ for the Next-Generation Deep-Ultraviolet Nonlinear Optical Materials. *Angew. Chem., Int. Ed.* **2018**, *57* (29), 8968−8972.

(14) Zou, G.; Huang, L.; Ye, N.; Lin, C.; Cheng, W.; Huang, H. $CsPbCO_3F$: A Strong Second-Harmonic Generation Material Derived from Enhancement via p-π Interaction. *J. Am. Chem. Soc.* **2013**, *135* (49), 18560−18566.

(15) Tran, T. T.; He, J.; Rondinelli, J. M.; Halasyamani, P. S. $RbMgCO_3F$: A New Beryllium-Free Deep-Ultraviolet Nonlinear Optical Material. *J. Am. Chem. Soc.* **2015**, *137* (33), 10504−10507.

(16) Huang, W.; Zhao, S.; Luo, J. Recent Development of Non-π-Conjugated Deep Ultraviolet Nonlinear Optical Materials. *Chem. Mater.* **2022**, *34* (1), 5−28.

(17) Wu, C.; Jiang, C.; Wei, G.; Jiang, X.; Wang, Z.; Lin, Z.; Huang, Z.; Humphrey, M. G.; Zhang, C. Toward Large Second-Harmonic Generation and Deep-UV Transparency in Strongly Electropositive Transition Metal Sulfates. *J. Am. Chem. Soc.* **2023**, *145* (5), 3040−3046.

(18) Mutailipu, M.; Han, J.; Li, Z.; Li, F.; Li, J.; Zhang, F.; Long, X.; Yang, Z.; Pan, S. Achieving the Full-Wavelength Phase-Matching for Efficient Nonlinear Optical Frequency Conversion in $C(NH_2)_3BF_4$. *Nat. Photonics* **2023**, *17*, 694−701.

(19) Liang, M. L.; Hu, C. L.; Kong, F.; Mao, J. G. $BiFSeO_3$: An Excellent SHG Material Designed by Aliovalent Substitution. *J. Am. Chem. Soc.* **2016**, *138* (30), 9433−9436.

(20) Mao, F.-F.; Hu, C.-L.; Xu, X.; Yan, D.; Yang, B.-P.; Mao, J.-G. $Bi(IO_3)F_2$: The First Metal Iodate Fluoride with a Very Strong Second Harmonic Generation Effect. *Angew. Chem., Int. Ed.* **2017**, *56* (8), 2151−2155.

(21) Nguyen, S. D.; Yeon, J.; Kim, S.-H.; Halasyamani, P. S. $BiO(IO_3)$: A New Polar Iodate That Exhibits an Aurivillius-Type $(Bi_2O_2)^{2+}$ Layer and a Large SHG Response. *J. Am. Chem. Soc.* **2011**, *133* (32), 12422−12425.

(22) Liang, M.-L.; Ma, Y.-X.; Hu, C.-L.; Kong, F.; Mao, J.-G. $Ba(MoO_2F)_2(QO_3)_2$ (Q = Se, Te): Partial Fluorination of MoO_6 Octahedra Enabling Two Polar Solids with Strong and Phase Matchable SHG Response. *Chem. Mater.* **2020**, *32* (22), 9688−9695.

(23) Gong, Y. P.; Hu, C. L.; Kong, F.; Mao, J. G. Exploration of New Birefringent Crystals in Bismuth d^0 Transition Metal Selenites. *Chem. - Eur. J.* **2019**, *25* (14), 3685−3694.

(24) Song, J. L.; Hu, C. L.; Xu, X.; Kong, F.; Mao, J. G. A Facile Synthetic Route to a New SHG Material with Two Types of Parallel π-Conjugated Planar Triangular Units. *Angew. Chem., Int. Ed.* **2015**, *54* (12), 3679−3682.

(25) Zhang, X. H.; Yang, B. P.; Chen, J.; Hu, C. L.; Fang, Z.; Wang, Z.; Mao, J. G. A New Iodate-Phosphate $Pb_2(IO_3)(PO_4)$ Achieving Great Improvement in Birefringence Activated by $(IO_3)^-$ Groups. *Chem. Commun.* **2020**, *56* (4), 635−638.

(26) Li, P.-F.; Hu, C.-L.; Kong, F.; Mao, J.-G. $Hg_2(SeO_3)(SO_4)$: The First Sulfate Selenite with Large Birefringence Explored from d^{10} Transition Metal Compounds. *Mater. Chem. Front.* **2022**, *6* (23), 3567−3576.

(27) Guo, J.; Tudi, A.; Han, S.; Yang, Z.; Pan, S. $Sn_2B_5O_9Cl$: A Material with Large Birefringence Enhancement Activated Prepared

via Alkaline-Earth-Metal Substitution by Tin. *Angew. Chem.* **2019**, *131* (49), 17839−17842.
(28) Li, P.-F.; Hu, C.-L.; Gong, Y.-P.; Kong, F.; Mao, J.-G. $Hg_3(Te_3O_8)(SO_4)$: A New Sulfate Tellurite with a Novel Structure and Large Birefringence Explored from d^{10} Metal Compounds. *Chem. Commun.* **2021**, *57* (57), 7039−7042.
(29) Han, Y.; Zhao, X.; Xu, F.; Li, B.; Ye, N.; Luo, M. $HgSO_4$: An Excellent Mid-Infrared Sulfate Nonlinear Optical Crystal with Wide Band Gap and Strong Second Harmonic Generation Response. *J. Alloys Compd.* **2022**, *902*, No. 163727.
(30) Qiu, H.; Li, F.; Jin, C.; Yang, Z.; Li, J.; Pan, S.; Mutailipu, M. Fluorination Strategy Towards Symmetry Breaking of Boron-centered Tetrahedron for Poly-fluorinated Optical Crystals. *Angew. Chem., Int. Ed.* **2024**, *63*, No. e202316194, DOI: 10.1002/anie.202316194.
(31) Qiu, H.; Li, F.; Li, Z.; Yang, Z.; Pan, S.; Mutailipu, M. Breaking the Inherent Interarrangement of $[B_3O_6]$ Clusters for Nonlinear Optics with Orbital Hybridization Enhancement. *J. Am. Chem. Soc.* **2023**, *145* (44), 24401−24407.
(32) Tian, H.; Lin, C.; Zhao, X.; Xu, F.; Wang, C.; Ye, N.; Luo, M. Ba(SO 3 CH 3) 2 : a Deep-Ultraviolet Transparent Crystal with Excellent Optical Nonlinearity Based on a New Polar Non-π-Conjugated NLO Building Unit SO_3CH_3. *CCS Chem.* **2022**, *5* (11), 2497−2505, DOI: 10.31635/ccschem.022.202202582.
(33) Parker, S. F.; Revill-Hivet, E. J.; Nye, D. W.; Gutmann, M. J. Structure and Vibrational Spectroscopy of Lithium and Potassium Methanesulfonates. *R. Soc. Open. Sci.* **2020**, *7* (7), No. 200776.
(34) Gernon, M. D.; Wu, M.; Buszta, T.; Janney, P. Environmental Benefits of Methanesulfonic Acid. *Green Chem.* **1999**, *1* (3), 127−140.
(35) Parker, S. F.; Zhong, L. Vibrational Spectroscopy of Metal Methanesulfonates: M = Na, Cs, Cu, Ag, Cd. *R. Soc. Open Sci.* **2018**, *5* (4), No. 171574.
(36) Guner, F. E. G.; Lutz, M.; Sakurai, T.; Spek, A. L.; Hondoh, T. Crystallization and Characterization of Magnesium Methanesulfonate Hydrate $Mg(CH_3SO_3)_2{\bullet}12H_2O$. *Cryst. Growth Des.* **2010**, *10*, 4327−4333.
(37) Wang, M.; Song, Z. G.; Jiang, H.; Gong, H. Thermal Decomposition of Metal Methanesulfonates in Air. *J. Therm. Anal. Calorim.* **2009**, *98* (3), 801−806.
(38) Đorđević, M.; Jeremić, D.; Kaluđerović, G. N.; Gómez-Ruiz, S.; Anđelković, B.; Radanović, D.; Brčeski, I. Synthesis and Spectroscopic Properties of Large Single-Crystals of Pb(II), Hg(II) and Sr(II) Methanesulfonato 1D Coordination Polymers. *Polyhedron* **2014**, *80*, 282−289.
(39) Preda, A. M.; Kitschke, P.; Rüffer, T.; Lang, H.; Mehring, M. Synthesis and Characterization of the Germanium Sulfonate Ge-$(CH_3SO_3)_2$ - a 3D Coordination Network Solid. *Z. Anorg. Allg. Chem.* **2016**, *642* (6), 467−471.
(40) Gagelmann, S.; Wickleder, M. S.; Fabian, M.; Klüner, T.; Langer, T.; Pöttgen, R. $Sn(CH_3SO_3)_2$: A Comprehensive Analysis. *Z. Anorg. Allg. Chem.* **2012**, *638* (10), 1580.
(41) Logemann, C.; Wickleder, M. S. The $[Au(CH_3SO_3)_4]^-$ Anion in the Crystal Structures of $M[Au(CH_3SO_3)_4]$ (M = Li, Na, Rb). *Z. Anorg. Allg. Chem.* **2012**, *638* (10), 1468−1472.
(42) Dolomanov, O. V.; Bourhis, L. J.; Gildea, R. J.; Howard, J. A. K.; Puschmann, H. OLEX2: A Complete Structure Solution, Refinement and Analysis Program. *J. Appl. Crystallogr.* **2009**, *42* (2), 339−341.
(43) Sheldrick, G. M. Crystal Structure Refinement with *SHELXL*. *Acta Crystallogr., Sect. C: Struct. Chem.* **2015**, *71* (1), 3−8.
(44) Mortensen, J. J.; Hansen, L. B.; Jacobsen, K. W. Real-Space Grid Implementation of the Projector Augmented Wave Method. *Phys. Rev. B* **2005**, *71* (3), No. 035109.
(45) Enkovaara, J.; Rostgaard, C.; Mortensen, J. J.; Chen, J.; Dułak, M.; Ferrighi, L.; Gavnholt, J.; Glinsvad, C.; Haikola, V.; Hansen, H. A.; Kristoffersen, H. H.; Kuisma, M.; Larsen, A. H.; Lehtovaara, L.; Ljungberg, M.; Lopez-Acevedo, O.; Moses, P. G.; Ojanen, J.; Olsen, T.; Petzold, V.; Romero, N. A.; Stausholm-Møller, J.; Strange, M.; Tritsaris, G. A.; Vanin, M.; Walter, M.; Hammer, B.; Häkkinen, H.; Madsen, G. K. H.; Nieminen, R. M.; Nørskov, J. K.; Puska, M.; Rantala, T. T.; Schiøtz, J.; Thygesen, K. S.; Jacobsen, K. W. Electronic Structure Calculations with GPAW: A Real-Space Implementation of the Projector Augmented-Wave Method. *J. Phys.: Condens. Matter* **2010**, *22* (25), No. 253202.
(46) Hjorth Larsen, A.; Jørgen Mortensen, J.; Blomqvist, J.; Castelli, I. E.; Christensen, R.; Dułak, M.; Friis, J.; Groves, M. N.; Hammer, B.; Hargus, C.; Hermes, E. D.; Jennings, P. C.; Bjerre Jensen, P.; Kermode, J.; Kitchin, J. R.; Leonhard Kolsbjerg, E.; Kubal, J.; Kaasbjerg, K.; Lysgaard, S.; Bergmann Maronsson, J.; Maxson, T.; Olsen, T.; Pastewka, L.; Peterson, A.; Rostgaard, C.; Schiøtz, J.; Schütt, O.; Strange, M.; Thygesen, K. S.; Vegge, T.; Vilhelmsen, L.; Walter, M.; Zeng, Z.; Jacobsen, K. W. The Atomic Simulation Environment—a Python Library for Working with Atoms. *J. Phys.: Condens. Matter* **2017**, *29* (27), No. 273002.
(47) Setyawan, W.; Curtarolo, S. High-Throughput Electronic Band Structure Calculations: Challenges and Tools. *Comput. Mater. Sci.* **2010**, *49* (2), 299−312.
(48) Lei, B. H.; Yang, Z.; Pan, S. Enhancing Optical Anisotropy of Crystals by Optimizing Bonding Electron Distribution in Anionic Groups. *Chem. Commun.* **2017**, *53*, 2818−2821.
(49) Lei, B. H.; Yang, Z.; Yu, H.; Cao, C.; Li, Z.; Hu, C.; Poeppelmeier, K. R.; Pan, S. Module-Guided Design Scheme for Deep-Ultraviolet Nonlinear Optical Materials. *J. Am. Chem. Soc.* **2018**, *140*, 10726−10733.
(50) Ok, K. M.; Bhuvanesh, N. S.; Halasyamani, P. S. Bi_2TeO_5: Synthesis, Structure, and Powder Second Harmonic Generation Properties. *Inorg. Chem.* **2001**, *40* (8), 1978−1980.
(51) Berdonosov, P. S.; Stefanovitch, S. Y.; Dolgikh, V. A. A New Bismuth-Selenium Oxychloride, $BiSeO_3Cl$: Crystal Structure and Dielectric and Nonlinear Optical Properties. *J. Solid State Chem.* **2000**, *149* (2), 236−241.
(52) Rademacher, O.; Göbel, H.; Oppermann, H. Crystal Structure of Bismuth Selenite, $Bi_2(SeO_3)_3$. *Z. Kristallogr. - New Cryst. Struct.* **2000**, *215*, 339−340.
(53) Brese, N. E.; O'Keeffe, M. Bond-Valence Parameters for Solids. *Acta Crystallogr., Sect. B: Struct. Sci.* **1991**, *47* (2), 192−197.
(54) Lozinšek, M.; Bunič, T.; Goreshnik, E.; Meden, A.; Tramšek, M.; Tavčar, G.; Žemva, B. Syntheses, Crystal Structures and Raman Spectra of $Ba(BF_4)(PF_6)$, $Ba(BF_4)(AsF_6)$ and $Ba_2(BF_4)_2(AsF_6)$-(H_3F_4); the First Examples of Metal Salts Containing Simultaneously Tetrahedral BF_4^- and Octahedral AF_6^- Anions. *J. Solid State Chem.* **2009**, *182* (10), 2897−2903.
(55) Radan, K.; Lozinšek, M.; Goreshnik, E.; Žemva, B. Syntheses, Structures and Raman Spectra of $Cd(BF_4)(AF_6)$ (A = Ta, Bi) Compounds. *J. Fluorine Chem.* **2011**, *132* (10), 767−771.
(56) Li, Y.; Wu, D.; Li, Z. R. Compounds of Superatom Clusters: Preferred Structures and Significant Nonlinear Optical Properties of the BLi_6-X (X = F, LiF_2, BeF_3, BF_4) Motifs. *Inorg. Chem.* **2008**, *47* (21), 9773−9778.
(57) Yang, H.; Li, Y.; Wu, D.; Li, Z. R. Structural Properties and Nonlinear Optical Responses of Superatom Compounds BF_4-M (M = Li, FLi_2, OLi_3, NLi_4). *Int. J. Quantum Chem.* **2012**, *112* (3), 770−778.
(58) Cao, J.; Wang, W. L.; Gao, L. J.; Fu, F. Mechanism and Thermodynamic Properties of CH_3SO_3 Decomposition. *Acta Phys. -Chim. Sin.* **2013**, *29* (6), 1161−1167.
(59) Liang, M. L.; Ma, Y. X.; Hu, C. L.; Kong, F.; Mao, J. G. $A(VO_2F)(SeO_3)$ (A = Sr, Ba) and $Ba(MOF_2)(TeO_4)$ (M = Mo, W): First Examples of Alkali-Earth Selenites/Tellurites with a Fluorinated D^0-TM Octahedron. *Dalton Trans.* **2018**, *47* (5), 1513−1519.
(60) Hämmer, M.; Brgoch, J.; Netzsch, P.; Höppe, H. A. The Role of the Bi^{3+} Lone Pair Effect in $Bi(H_3O)(SO_4)_2$, $Bi(HSO_4)_3$, and $Bi_2(SO_4)_3$. *Inorg. Chem.* **2022**, *61* (9), 4102−4113.
(61) Lee, E. P.; Song, S. Y.; Lee, D. W.; Ok, K. M. New Bismuth Selenium Oxides: Syntheses, Structures, and Characterizations of Centrosymmetric $Bi_2(SeO_3)_2(SeO_4)$ and $Bi_2(TeO_3)_2(SeO_4)$ and Noncentrosymmetric $Bi(SeO_3)(HSeO_3)$. *Inorg. Chem.* **2013**, *52* (7), 4097−4103.
(62) Bonadeo, H.; Silberman, E. Infrared Studies on BF_4^- in Alkali Halide Solid Solutions. *J. Mol. Spectrosc.* **1969**, *32*, 214−221.

https://doi.org/10.1021/acs.chemmater.3c03278
Chem. Mater. XXXX, XXX, XXX−XXX

(63) Nigoghossian, K.; Miyashita, T.; Omura, A.; Yeroslavsky, G.; Kim Dung, D. T.; Okubo, K.; Umezawa, M.; Kamimura, M.; Soga, K. Infrared to Visible Upconversion Luminescence of Trivalent Erbium Tetrafluoroborate Complexes. *Opt. Mater. Express* **2020**, *10* (7), 1749−1766.
(64) Fang, C.; Li, W. F.; Koster, R. S.; Klimeš, J.; Blaaderen, A.; Huis, M. A. The Accurate Calculation of the Band Gap of Liquid Water by Means of GW Corrections Applied to Plane-wave Density Functional Theory Molecular Dynamics Simulations. *Phys. Chem. Chem. Phys.* **2015**, *17*, 365−375.
(65) Xu, X.; Li, B.; Li, H. Native O and Se Vacancy Defects in Bi_2O_5Se, $Bi_2O_9Se_3$, and $Bi_2O_{10}Se_3$ Dielectrics for Nanoelectronics. *Phys. Status Solidi RRL* **2021**, *15* (2), No. 2000540.
(66) Song, J. L.; Qian, C. Syntheses, Crystal Structures, and Properties of Two Quaternary Selenite/Tellurite-Nitrates with Formula of $Bi(SeO_3)(NO_3)$ and $Bi_3(\mu_3\text{-}OH)(TeO_3)_3(NO_3)_2$. *ChemistrySelect* **2017**, *2* (4), 1681−1685.
(67) Meng, C. Y.; Wei, M. F.; Geng, L.; Hu, P. Q.; Yu, M. X.; Cheng, W. D. Synthesis, Structure, and Characterization of Two New Bismuth(III) Selenite/Tellurite Nitrates: $[(Bi_3O_2)(SeO_3)_2](NO_3)$ and $[Bi(TeO_3)](NO_3)$. *J. Solid State Chem.* **2016**, *239*, 46−52.
(68) Shi, S.; Lin, C.; Yang, G.; Cao, L.; Li, B.; Yan, T.; Luo, M.; Ye, N. $A_2Bi_2(SeO_3)_3F_2$ (A = K and Rb): Excellent Mid-Infrared Nonlinear Optical Materials with Both Strong SHG Responses and Large Band Gaps. *Chem. Mater.* **2020**, *32* (18), 7958−7964.
(69) Chung, J. Y.; Jo, H.; Yeon, S.; Byun, H. R.; You, T.-S.; Jang, J. I.; Ok, K. M. $Bi_3(SeO_3)_3(Se_2O_5)F$: A Polar Bismuth Selenite Fluoride with Polyhedra of Highly Distortive Lone Pair Cations and Strong Second-Harmonic Generation Response. *Chem. Mater.* **2020**, *32* (17), 7318−7326.
(70) Tang, R. L.; Hu, C. L.; Xie, W. J.; Huang, Q. M.; Mao, J. G. $Bi_2[B_2(SeO_3)_6]$: A Metal Boroselenite with a Unique Zero-Dimensional $[B_2(SeO_3)_6]^{6-}$ Anionic Group and Large Birefringence. *Inorg. Chem.* **2021**, *60* (6), 3539−3542.
(71) Gong, Y. P.; Hu, C. L.; Kong, F.; Mao, J. G. Exploration of New Birefringent Crystals in Bismuth d^0 Transition Metal Selenites. *Chem. - Eur. J.* **2019**, *25* (14), 3685−3694.
(72) Sun, C.; Mei, D.; Xu, J.; Wu, Y. Hydrothermal Synthesis, Crystal Structures, and Optical Properties of $H[Bi_3O(Te_3O_9)](NO_3)_2$ and $[Bi_2(TeO_3)_2](SO_4)$. *J. Alloys Compd.* **2017**, *702*, 410−417.
(73) Chung, J. Y.; Yeon, S.; Ryu, H.; You, T.-S.; Jang, J. I.; Ok, K. M. Nonlinear Optical Properties of a New Polar Bismuth Tellurium Oxide Fluoride, $Bi_3F(TeO_3)(TeO_2F_2)_3$. *J. Alloys Compd.* **2022**, *895*, No. 162603.
(74) Sun, J.; Wu, Z.; Lee, M. H.; Duan, H. A Theoretical Perspective to Study the Optical Properties of Tetrafluoroborates. *ChemPhysChem* **2022**, *23* (15), No. 202200205.
(75) Mohammed, S. A. S.; Yahya, W. Z. N.; Bustam, M. A.; Kibria, M. G. Experimental and Computational Evaluation of 1,2,4-Triazolium-Based Ionic Liquids for Carbon Dioxide Capture. *Separations* **2023**, *10* (3), No. 192, DOI: 10.3390/separations10030192.

https://doi.org/10.1021/acs.chemmater.3c03278
Chem. Mater. XXXX, XXX, XXX−XXX